Magnus Forces on Spinning Supersonic Cones. Part II: Inviscid Flow

B. R. Sanders*
Sandia Laboratories, Livermore, Calif.
and
H. A. Dwyer†
University of California-Davis, Davis, Calif.

The numerical solution of steady, three-dimensional, inviscid, supersonic flows is applied to the calculation of Magnus forces on spinning cones at angle of attack. The Magnus force is made up of several contributions. The contribution of the asymmetrical boundary-layer displacement-thickness interaction with the inviscid flowfield is considered here. Three-dimensional, laminar boundary-layer solutions for the spinning cone were obtained by methods described in Part I of this paper. The displacement-thickness contribution to the Magnus force is calculated by solving the complete inviscid flowfield over body shapes obtained by adding the three-dimensional displacement thickness to the cone radius. The gasdynamic equations are solved by applying MacCormack's second-order shock-capturing finite-difference technique. Special precautions had to be taken, in both finite-differencing and in applying the surface boundary conditions, to maintain enough significant digits in the pressure calculation, since the Magnus force is as small as one part in 300 of the normal force for some cases considered. The displacement-thickness contribution to the Magnus force, along with three other contributions described in Part I of this paper, are summarized here in Part II. The considerable cancellation effect observed among the four contributions shows that all of the components must be included if accurate predictions of the Magnus force are to be obtained.

Introduction

THE Magnus force is the small force at right angles to the lift vector on spinning, axisymmetric bodies at angle of attack, and arises purely because of viscosity in the flowfield around the body. The physical phenomena resulting in a Magnus (side) force on spinning bodies have been postulated by several authors. Sedney[1] was the first to test the hypothesis that the Magnus force on slender bodies at small angle of attack is caused by the displacement effect of the boundary layer. Sedney obtained a regular perturbation solution to the boundary-layer equations for a spinning cone, and with the aid of slender-body theory, was able to show a significant side force caused by displacement-thickness interaction with the inviscid flowfield.

More recent research has shown that there are at least four significant contributions to the small Magnus force for the case of laminar flow.[2,3] Both separated and transitioned flows give rise to large Magnus forces, but these flows will not be considered here. The Magnus force contributions which have been identified are a centrifugal pressure gradient caused by the spin-induced rotation of the boundary layer, two asymmetrical shear stress distributions on the body, and an asymmetrical pressure distribution caused by displacement-thickness interaction with the inviscid flowfield. The extreme smallness of all of the Magnus force contributions (on the order of less than 1% of the normal force) makes their calculation a difficult task. In addition, because spin destroys all symmetry in the flowfield, three-dimensional calculations are required, both in the boundary layer and the inviscid outer-flow solutions.

Submitted May 25, 1975; revision received Aug. 26, 1975. This work was partially supported by the U.S. Energy Research and Development Administration, Contract No. AT-(29-1)-789.

Index categories: Supersonic and Hypersonic Flow; Boundary Layers and Convective Heat Transfer – Laminar.

*Member of the Technical Staff, Combustion Research Division 8115. Member AIAA.

†Professor, Department of Mechanical Engineering. Member AIAA.

The major contribution to the Magnus force is that of a spin-induced asymmetry of the boundary layer. Previous calculations of the displacement-thickness contribution have been approximate, since slender-body theory has been used to estimate the pressure distribution over the new body shape.[1,3,4] There are several basic inaccuracies built into this approach. For one, slender-body theory is, strictly speaking, applicable only to very slender shapes whose maximum body thickness is small compared with the length; and for many body shapes of interest, this assumption is not satisfied. For another, this type of analysis is based on a linearized version of the compressible flow equations.

This paper describes a method of calculating the displacement-thickness contribution to the Magnus force on cones in an exact manner by solving completely the inviscid flowfield over a shape composed of the cone plus boundary-layer displacement thickness. The full inviscid equations are solved by using a modification of MacCormack's[5-7] second-order method to march from the tip of the new shape to the end. The bow shock is captured by means of the numerical routine, and the surface tangency condition is imposed by Abbett's Euler-predictor/simple-wave-corrector method.[8] Starting conditions are obtained by calculating a conical flowfield solution near the tip, where the boundary-layer displacement thickness is so small that it can be neglected. This technique is very general and, so long as the flowfield is supersonic, can handle almost any body shape, for example, an ogive-cylinder. Special numerical precautions have to be taken in this problem since the displacement-thickness contribution to the Magnus force may be as small as one part in 300 of the normal force. It will be shown that truncation and roundoff errors, though they be of aceptable magnitude for most flowfield solutions, can destroy completely any significance in the calculation of the small Magnus forces.

Part I of this two-part paper discusses the shear stress and radial pressure gradient contributions to the Magnus force for a set of Mach numbers, wall temperatures, angles of attack, and spin rates. Part II summarizes the displacement-thickness contribution and discusses the total Magnus force predictions from all four contributions. The results show that a com-

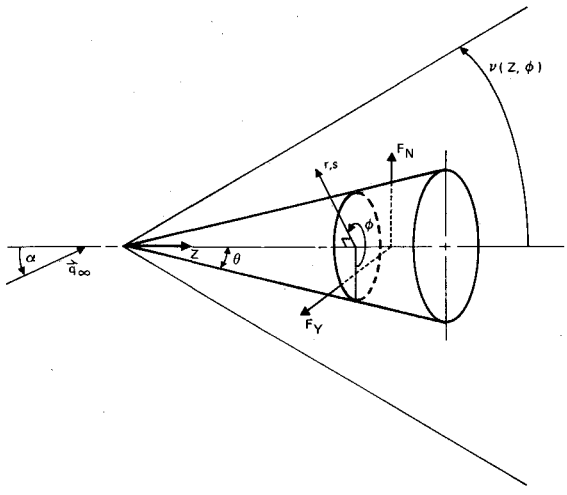

Fig. 1 Cylindrical coordinate system for cone at angle of attack.

parison of the total Magnus force with that predicted by two previously reported methods is in good circumstantial agreement, but there is considerable disagreement among predictions for the various components of that force.

Governing Equations

For most three-dimensional body shapes, cylindrical coordinates are a convenient system for solving the inviscid gasdynamic equations. Figure 1 shows the coordinate scheme for a cone at angle of attack. Here, θ represents the cone half-angle, ν gives the bow shock angle, and F_N and F_Y are, respectively, the normal and Magnus side forces.

The steady gasdynamic equations of inviscid flow in dimensionless, conservation-law form can be written as a single vector equation as follows:

$$(\partial\tilde{E}/\partial Z)+\partial\tilde{F}/\partial r)+(\partial\tilde{G}/\partial\phi)+\tilde{H}=0) \tag{1}$$

where the four-dimensional vectors are defined by

$$\tilde{E}=\begin{vmatrix}\tilde{\rho}\tilde{u}\\ K\tilde{P}+\tilde{\rho}\tilde{u}^2\\ \tilde{\rho}\tilde{u}\tilde{v}\\ \tilde{\rho}\tilde{u}\tilde{v}\end{vmatrix},\quad \tilde{F}=\begin{vmatrix}\tilde{\rho}\tilde{v}\\ \tilde{\rho}\tilde{u}\tilde{v}\\ K\tilde{P}+\tilde{\rho}\tilde{v}^2\\ \tilde{\rho}\tilde{u}\tilde{v}\end{vmatrix}$$

$$\tilde{G}=1/r\begin{vmatrix}\tilde{\rho}\tilde{w}\\ \tilde{\rho}\tilde{u}\tilde{w}\\ \tilde{\rho}\tilde{v}\tilde{w}\\ K\tilde{P}+\tilde{\rho}\tilde{w}^2\end{vmatrix},\quad \tilde{H}=1/r\begin{vmatrix}\tilde{\rho}\tilde{v}\\ \tilde{\rho}\tilde{u}\tilde{v}\\ \tilde{\rho}(\tilde{v}^2-\tilde{w}^2)\\ 2\tilde{\rho}\tilde{v}\tilde{w}\end{vmatrix}$$

The nondimensional velocity components $\tilde{u}$, $\tilde{v}$, and $\tilde{w}$ are along the coordinate directions Z, r, and ϕ, respectively. The first row represents the continuity equation, and the second, third, and fourth rows represent, respectively, the Z, r, and ϕ momentum equations. Here, the density has been made dimensionless with respect to freestream total density; the pressure, by freestream total pressure; and all velocity components, by the maximum adiabatic velocity; and K is defined as

$$K=(\gamma-1)/2\gamma$$

An integrated form of the energy equation can be substituted for the differential form in the absence of heat addition, body forces, and unsteady effects. This equation, in dimensionless form, is

$$\tilde{P}=\tilde{\rho}(1-\tilde{u}^2-\tilde{v}^2-\tilde{w}^2) \tag{2}$$

Coordinate Transformation

A convenient coordinate transformation which normalizes the coordinate distance in the radial direction between the surface and the outer boundary is[5]

$$Z'=Z,\quad \phi'=\phi,\quad s=(r-r_b)/(r_{ob}-r_b)$$

where

$r_b=r_b(Z,\phi)$ = body radius in cylindrical coordinates
$r_{ob}=r_{ob}(Z,\phi)$ = outer computational boundary radius in cylindrical coordinates

Applying this set of nonorthogonal coordinate transformations to Eq. (1) gives the following form:

$$(\partial E/\partial Z)+(\partial F/\partial s)+(\partial G/\partial\phi)+H=0 \tag{3}$$

where

$$E=\tilde{E},\quad F=\tilde{E}\frac{\partial s}{\partial z}+\tilde{F}\frac{\partial s}{\partial r}+\tilde{G}\frac{\partial s}{\partial\phi}$$

$$G=\tilde{G},\quad H=\tilde{H}-\tilde{E}\frac{\partial}{\partial s}\left(\frac{\partial s}{\partial Z}\right)-\tilde{F}\frac{\partial}{\partial s}\left(\frac{\partial s}{\partial r}\right)-\tilde{G}\frac{\partial}{\partial s}\left(\frac{\partial s}{\partial\phi}\right)$$

The solution of Eq. (3) poses an initial value problem, which is hyperbolic in the Z coordinate. A grid mesh is set up in the (s,ϕ) plane, with constant grid spacing Δs and $\Delta\phi$. An initial data plane is specified by assuming either freestream conditions or conditions from some other computation; and, with the specification of the body and outer-boundary geometry, the solution is advanced in the direction of increasing Z. The step size in the Z direction is determined by the slope of the characteristic lines, and the inviscid tangent-flow boundary condition is enforced at the solid surface. The outer computational boundary is selected so that all shocks and disturbances are contained between the boundary and the body surface. With the outer boundary specified in this way, the outer boundary conditions become merely the freestream conditions.

Finite-Difference Methods and Equations

For the solution of Eq. (3), a second-order, two-step method is used. The method, that of MacCormack,[5-7] employs a Euler predictor and a modified Euler corrector. The basic flow equation in vector form, Eq. (3), is

$$(\partial E/\partial Z)+(\partial F/\partial s)+(\partial G/\partial\phi)+H=0$$

The grid mesh is denoted as (s_i,ϕ_j), with constant spacing Δs and $\Delta\phi$. Variables at a known data plane are represented by a superscript n, and this Z position defines the Z^n plane. The superscript (1) denotes quantities which have been evaluated in the $Z^n+\Delta Z$ plane after application of the predictor but before the corrector has been applied. And finally, the superscript $n+1$ represents the final solution in the $Z^n+\Delta Z$ plane after both the predictor and corrector steps have been applied.

Applying forward differences in all three space dimensions in Eq. (3) and solving for $E^{(1)}_{i,j}$ gives the predictor equation:

$$E^{(1)}_{i,j}=E^n_{i,j}-(\Delta Z/\Delta s)(F^n_{i+1,j}-F^n_{i,j})$$
$$-(\Delta Z/\Delta\phi)(G^n_{i,j+1}-G^n_{i,j})-\Delta ZH^n_{i,j} \tag{4}$$

Applying backward spatial differences in the s and ϕ directions gives, for the corrector equation

$$E_{i,j}^{n+1} = \tfrac{1}{2}(E_{i,j}^{(1)} E_{i,j}^{n}) - \tfrac{1}{2}\{ (\Delta Z/\Delta s)(F_{i,j}^{(1)} - F_{i-1,j}^{(1)}) + (\Delta Z/\Delta\phi)(G_{i,j}^{(1)} - G_{i,j-1}^{(1)}) + \Delta Z H_{i,j}^{(1)} \} \quad (5)$$

The use of two forward and two backward spatial differences is not unique to this method. The spatial derivatives may be permuted in any of four ways: 1) two forward and two backward differences; 2) two backward and two forward differences; 3) one forward and one backward, followed by one backward and one forward; and 4) one backward and one forward, followed by one forward and one backward. Kutler et al.[5] give a concise method of writing the finite-difference equations so that methods 1-4 can be selected at will:

Predictor

$$E_{i,j}^{(1)} = E_{i,j}^{n} - \{ (\Delta Z/\Delta s)[(1-\epsilon_s)F_{i+1,j}^{n} - (1-2\epsilon_s)F_{i,j}^{n} - \epsilon_s F_{i-1,j}^{n}] + (\Delta Z/\Delta\phi)[(1-\epsilon_\phi)G_{i,j+1}^{n} - (1-2\epsilon_\phi)G^{n}{}_{i,j} - \epsilon_\phi G_{i,j-1}^{n}] + \Delta Z H_{i,j}^{n} \} \quad (6)$$

Corrector

$$E_{i,j}^{n+1} = \tfrac{1}{2}(E_{i,j}^{n} + E_{i,j}^{(1)}) - \tfrac{1}{2}\{ (\Delta Z/\Delta s)[\epsilon_s F_{i+1,j}^{(1)} + (1-2\epsilon_s)F_{i,j}^{(1)} + (\epsilon_s - 1)F_{i-1,j}^{(1)}] + (\Delta Z/\Delta\phi)[\epsilon_\phi G_{i,j+1}^{(1)} + (1-2\epsilon_\phi)G_{i,j}^{(1)} + (\epsilon_\phi - 1)G_{i,j-1}^{(1)}] + \Delta Z H_{i,j}^{(1)} \} \quad (7)$$

Then the schemes are selected by 1) $\epsilon_s = 0$, $\epsilon_\phi = 0$; 2) $\epsilon_s = 1$, $\epsilon_\phi = 1$; 3) $\epsilon_s = 0$, $\epsilon_\phi = 1$; and 4) $\epsilon_s = 1$, $\epsilon_\phi = 0$.

MacCormack[6] has suggested that, for general flow problems, a cyclic permutation of the four differencing methods would produce unbiased results. Figure 2 shows the computational grid in the $s-\phi$ plane. It is clear that applying a forward or backward difference in the ϕ direction at point b will produce different derivative information since there is a strong pressure gradient from windward (0°) to leeward (180°) sides of a cone at angle of attack. The same is true for the first-order finite differences in the s direction. Each of the four finite-difference schemes just listed will use different physical derivative information at each point and will give a different flowfield result. In the present problem, a cyclic permutation of the four differencing methods causes a cyclic change in the body surface pressure great enough to overshadow completely the surface pressure changes caused by the addition of a boundary layer to the cone. The flowfield for a cone at angle of attack and without a boundary layer is symmetrical about the 0°-180° plane. If the finite differencing of method 1 is used all the way from 0° to 360°, the resulting solution will no longer be symmetrical about the 0°-180° line. Trial calculations were made, with method 1 applied all the way around the cone, and the result was a net side force of the same order of magnitude as that of the Magnus force. This value represents an inherent error in side force since, because a plane of symmetry is present, the cone solution theoretically has no net side force. When the finite differencing was performed with method 1 for $0<\phi<180$ and method 2 for $180<\phi<360$, the net side force coefficient on the cone was on the order of 10^{-8}. This value of side force is caused by round-off error in the CDC 6600 computer. With an expected Magnus force coefficient of 10^{-3}, the special precautions taken in the finite-differencing have reduced the inherent side force error to a value five orders of magnitude smaller than the effect which is being sought.

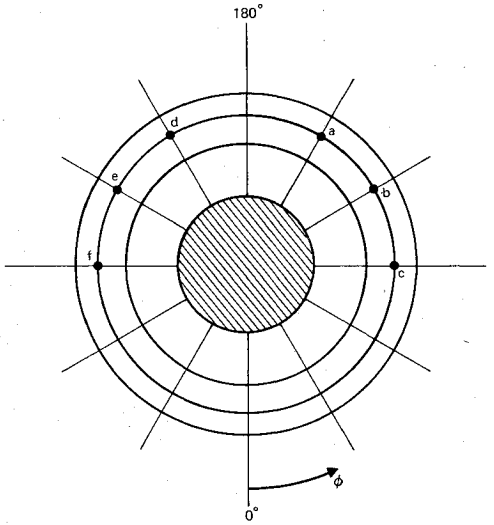

Fig. 2 Computational grid in physical coordinates.

Modifications have been made to the differencing scheme at the cone surface and in the windward and leeward planes. By physical constraint, the s derivatives in both the predictor and the corrector must be approximated with forward differences on the cone surface. In addition, central differences are applied for the ϕ derivatives everywhere on the cone surface and at all grid points in the windward and leeward planes. The central ϕ differences in the windward and leeward planes help preserve the natural symmetry in the flowfield and give a much better representation of the derivatives in the symmetry plane. Central ϕ differences on the surface ($i=1$) are used to provide data smoothing for bodies which must be specified by a finite number of surface points, rather than by an algebraic expression.

Initial Conditions

Near the tip of a spinning cone, the boundary layer is almost symmetrical; therefore, there is very little contribution to the Magnus force from the tip portion of the body. All of the Magnus results presented in this paper are for calculations which are begun from a cone solution at 0.01 ft downstream of the cone tip. The conical starting conditions are obtained by initializing with freestream conditions over the entire starting plane and iterating until the solution reaches an acceptable level of convergence.

The Magnus force calculations use eight different solutions as starting conditions, and these eight cases are compared in Table 1 with the cone surface pressure results of Jones.[9] Each of the Mach 2 and 4 cases is calculated with a grid of 15×36 and for 150 iterations, beginning with freestream conditions. The Mach 1.5 cases could not be started with freestream variables; instead, they first are converged iteratively by starting a Mach 1.9 case with the converged solution of Mach 2.0. The solution for Mach 1.9 then is used to initialize a case of Mach 1.8, and this procedure is continued until cases for Mach 1.5 are obtained. All of the Mach 1.5 cases are computed with a grid of 30×36.

Boundary Conditions

The appropriate inviscid boundary condition at a solid surface is that there is no velocity component normal to the surface. Mathematically, this condition, which applies over the entire surface, is expressed as

$$\boldsymbol{q}\cdot\boldsymbol{n}_b = 0$$

where $\boldsymbol{q}$ is the total velocity and $\boldsymbol{n}_b$ the surface unit normal vector.

There are numerous techniques available for enforcing, at least in an approximate manner, the velocity tangency condition in inviscid, supersonic flows. Abbett[8] has devised a Euler-predictor/simple-wave-corrector (EP/SWC) method, which is both simple and accurate, for two-dimensional flows.

Table 1 Surface pressure comparison, 10° cone

		P/P_∞, present analysis			P/P_∞, Jones[9]		
M_∞	α	0°	90°	180°	0°	90°	180°
1.5	2.0	1.2250	1.1863	1.1586	1.2329	1.1906	1.1613
1.5	4.0	1.2585	1.1706	1.1277	1.2752	1.1774	1.1318
2.0	2.0	1.3518	1.2802	1.2291	1.3596	1.2861	1.2338
2.0	4.0	1.4242	1.2606	1.1788	1.4355	1.2669	1.1832
2.0	6.0	1.5055	1.2287	1.1354	1.5205	1.2350	1.1402
4.0	2.0	2.1626	1.8737	1.6548	2.1651	1.8764	1.6575
4.0	4.0	2.4805	1.8363	1.4648	2.4860	1.8392	1.4672
4.0	6.0	2.8432	1.7764	1.3107	2.8520	1.7819	1.3145

Kutler et al.[5] have applied Abbett's scheme in three dimensions to a problem with severe changes in body shape and slope. Kutler and co-workers claim that the method has good accuracy and is simple to use. The EP/SWC method consists of using a Euler predictor scheme to predict the flow variables at the new computational plane. The velocity vector obtained from the predicted velocity components generally will not be tangent to the surface. The surface tangency condition then is enforced by turning the velocity vector through the angle required to bring it exactly parallel with the surface. The method of turning the velocity vector is to use either an isentropic expansion or an isentropic compression, whichever is required.

The boundary condition is applied in two distinct steps. First, a Euler predictor is used to predict values $\tilde{P},\tilde{\rho},\tilde{u},\tilde{v}$, and w on the surface at the station $Z^{n+1}=Z^n+\Delta Z$. Second, a simple isentropic expansion or compression is used to force the solution to match the surface tangency condition. The following difference scheme is applied to the predictor, Eq. (6), at the body:

$$E^{(1)}_{i,j}E^n_{i,j}-(\Delta Z/\Delta s)\left[F^n_{2,j}-F^n_{1,j}\right](-\Delta Z/\Delta s)\left[(1-\epsilon_\phi)G^n_{1,j+1}-(1-2\epsilon_\phi)G^n_{1,j}-\epsilon_\phi G^n_{1,j-1}\right]+\Delta Z H^n_{1,j} \tag{8}$$

The derivative $\partial F/\partial s$ has been replaced by a first-order forward (in positive s direction) finite difference. The derivative $\partial G/\partial\phi$ is selected as a second-order central difference, a first-order forward difference, or a first-order backward difference, the choice depending on the value assigned to ϵ_ϕ.

In the present study, the boundary condition scheme is modified in that the corrector step is retained and the boundary condition applied after both the predictor and corrector have been applied. The modified corrector scheme used was

$$E^{n+1}_{1,j}=\tfrac{1}{2}\left(E^n_{1,j}+E^{(1)}_{1,j}\right)-\tfrac{1}{2}\{(\Delta Z/\Delta s)\left[F^{(1)}_{2,j}-F^{(1)}_{1,j}\right]+(\Delta Z/\Delta\phi)\left[\epsilon_\phi G^{(1)}_{1,j+1}+(1-2\epsilon_\phi)G^{(1)}_{1,j}+(\epsilon_\phi-1)G^{(1)}_{1,j-1}\right]+\Delta Z H^{(1)}_{1,j}\} \tag{9}$$

Again, the derivative $\partial F/\partial s$ has been replaced by a forward difference (away from the surface); and the option of central, forward, or backward differences is selected on the basis of the value of ϵ_ϕ. For the present problem, central differences are used in the ϕ direction at the surface.

The outer computational boundary must lie outside all shocks in the flowfield. In practice, the outer boundary is specified so that at least two radial grid points are positioned in the freestream. The outermost radial grid points are given freestream values, and these points are not integrated in the finite-difference routine.

Magnus Force Calculations

Three of the four contributions to the Magnus force can be calculated directly from the three-dimensional boundary-layer solution for the spinning cone. These three are the wall shear components τ_ϕ and τ_x and the radial pressure gradient δP. The fourth contribution, that due to the displacement thickness, must be calculated separately by considering the interaction of the boundary layer with the inviscid flowfield. Boundary-layer displacement-thickness distributions for a spinning cone at angle of attack, calculated by a method described in Part I of this paper, are added to the cone, thereby defining a new three-dimensional body which no longer has a plane of symmetry. The surface pressure distribution resulting from a complete inviscid flowfield solution about the new body shape enables a direct calculation of the boundary-layer displacement-thickness contribution to the Magnus force. This approach uses no simplifying assumptions in the supersonic theory, and thus is an exact calculation of the displacement-thickness contribution.

Before presenting the Magnus force results for a series of flow conditions, one of the cases will be discussed thoroughly to make clear the procedures used in calculating the displacement-thickness contribution and to offer an interpretation of the detailed results. The case to be discussed is that of a cone with a 10° half-angle and a 2° angle of attack in a supersonic flow of Mach number equal to 2. The boundary-layer calculations were performed for a freestream Reynolds number of 1.405×10^6 based on a length of 1 ft and a spin rate of 30,000 rpm for a ratio of cone surface to freestream stagnation temperature of $T_w/T_0=0.56$. The boundary-layer solution, described in Part I of this paper, provides the two-dimensional displacement thicknesses δ_x and δ_ϕ, from which the three-dimensional displacement thickness, Δ, can be calculated.

These values of Δ are added to the cone radius, which then describes the new body surface of cone plus displacement thickness. The integration of the inviscid equations, Eq. (3), requires the values of the body derivatives $\partial r_b/\partial Z$ and $\partial r_b/\partial\phi$. These were obtained by a second-order numerical differentiation. The magnitude of the r_{b_ϕ} derivative is quite small, but the effects of this derivative are significant and cannot be ignored. The primary contribution to the surface pressure comes from the r_{b_z} derivative. This relationship can be seen if one considers a right circular cone at angle of attack in a supersonic stream. The surface pressure, as well as all other flow variables, depends not on the radius of the cone, but on the slope of its surface [$r_{b_z}=\tan(\theta)$ for a cone of half angle θ].

The displacement-thickness contribution to the Magnus force arises from the pressure difference from one side of the body to the other. Although the pressure difference is being calculated on a body made up of cone plus displacement thickness, the correct value of the net side force comes from considering that the pressure on the new body shape is acting on the surface of the cone. This interpretation of the Magnus force is consistent with the boundary-layer approximation, which is that the pressure outside the thin boundary layer is constant through that boundary layer. Since the pressure differences between the two sides of the body are quite small, it is convenient to subtract corresponding pressures [$\tilde{P}(\tilde{\phi})-\tilde{P}(360°-\phi)$] in order to make the differences visible. Actually, the pressure difference defined in this way is a meaningful parameter, because this quantity arises naturally

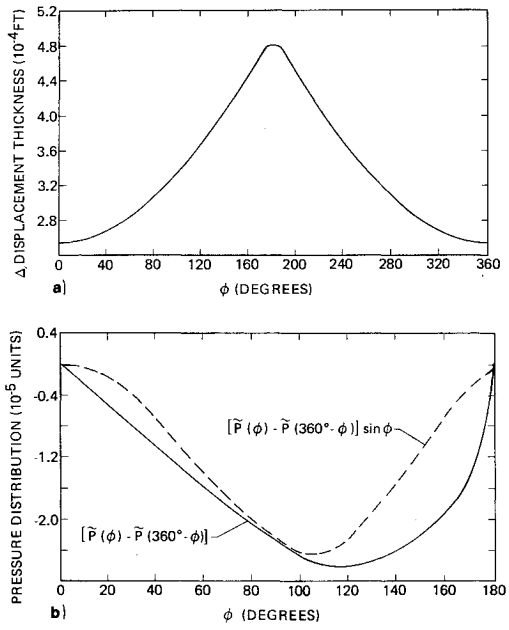

Fig. 3 Geometry and pressure distribution at 0.1 ft from the tip ($M_\infty = 2.0$, $\alpha = 2.0°$, $R_{e_\infty} = 1.405 \times 10^6$, $\omega = 30{,}000$ rpm, $T_w/T_0 = 0.56$); a) Three-dimensional displacement thickness; b) Distribution of surface pressure.

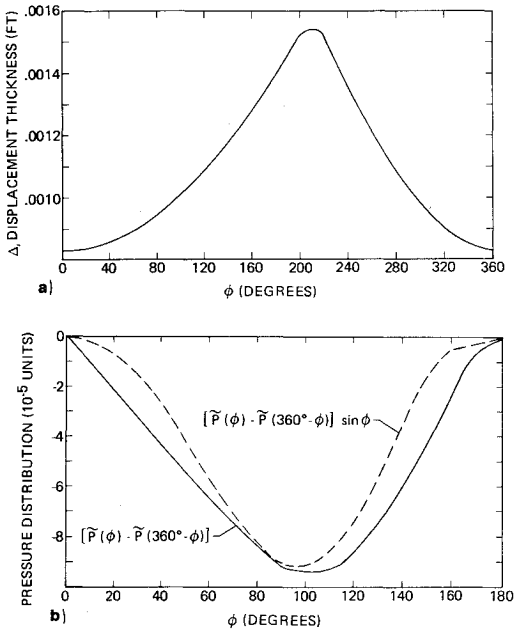

Fig. 4 Geometry and pressure distribution at 1.0 ft from the tip ($M_\infty = 2.0$, $\alpha = 2.0°$, $R_{e_\infty} = 1.405 \times 10^6$, $\omega = 30{,}000$ rpm, $T_w/T_0 = 0.56$): a) Three-dimensional displacement thickness; b) Distribution of surface pressure.

in the Magnus force integral.

Figures 3 and 4 are plots of the boundary-layer displacement thicknesses and pressure differences for the example case. The figures show the development of the solution at 0.1 ft and 1.0 ft. Figure 3a shows the three-dimensional boundary-layer displacement thickness around the cone at 0.1 ft from the tip. At this position on the cone, spin has produced only a small asymmetry in displacement thickness. Figure 3b shows the pressure distribution that results from adding the boundary layer to the cone body. The solid curve shows the plot of $\tilde{P}(\phi) - \tilde{P}(360° - \phi)$ as a function of body angle ϕ. The dashed curve is the solid curve multiplied by $\sin(\phi)$; therefore, the dashed curve is proportional to the contribution to the Magnus force.

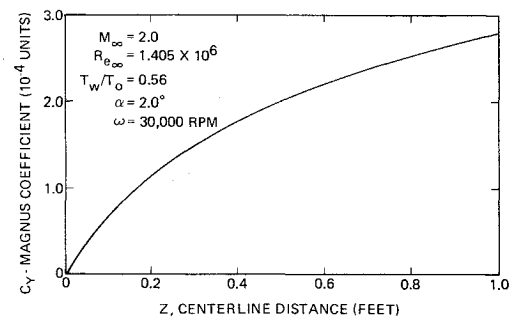

Fig. 5 Magnus force coefficient as a function of centerline distance for a 10° cone.

At 1.0 ft down the cone, spin has produced a considerable boundary-layer asymmetry, as shown in Fig. 4a. Here, the maximum displacement thickness has moved from the leeward plane to the 210° position. This increased body asymmetry results in a much greater pressure distribution, as shown in Fig. 4b.

Figure 5 gives the Magnus force coefficient as a function of distance down the body. This curve means that, if the body were cut off at any Z position, the Magnus coefficient would apply to a body of that length. Although the normal and axial force coefficients for a cone are independent of position on the body, the same is not true for the Magnus force caused by displacement thickness. The boundary-layer displacement thickness is affected by the surface velocity of the cone, not by angular velocity. The surface velocity increases linearly with Z, and the boundary layer becomes increasingly less symmetrical. Near the tip of the body, where the surface velocity is small, the displacement thickness is almost symmetrical. Figure 3a shows that, at $Z = 0.1$ ft, the boundary-layer displacement-thickness maximum is still at 180°. But at $Z = 1.0$ ft, where the surface velocity is 10 times larger than at 0.1, Fig. 4a shows that the displacement thickness maximum has moved to 210°.

It was mentioned at the beginning of this section that the magnitude of r_{b_ϕ} was small but could not be ignored. A case exactly like the one just described was calculated with r_{b_ϕ} set equal to zero everywhere. The net result was a prediction of C_Y of 0.375×10^{-3} at $Z = 1.0$ ft, as opposed to the value of 0.290×10^{-3} from Fig. 5. The difference, when $r_{b_\phi} = 0.0$ is assumed, is an increase in Magnus coefficient of nearly 30%. The physical significance of setting r_{b_ϕ} equal to zero is that the numerical routine sees a tangent cone at each position on the body. Any numerical or analytical method which employs a tangent cone approximation when there is body curvature in the plane of $Z = \text{const}$ will be making a significant error solely because of the curvature effect.

Results

Many authors have considered the calculation of Magnus force coefficients for spinning cones. Sedney[1] has performed a regular perturbation expansion and series solution of the boundary-layer equations based on spin rate and angle of attack. His solution provided the boundary-layer displacement thickness, from which he calculated a Magnus force contribution using slender-body theory. Sedney did not consider any other contributions such as wall shear and radial pressure gradient.

Vaughn and Reis[4] have developed an approximate analytical method of predicting Magnus forces for axisymmetric body shapes with both laminar and turbulent flow. They considered two components of the Magnus force, namely, those due to radial pressure gradient and displacement thickness.

Table 2 shows the comparison of the solutions by Sedney,[1] by Vaughn and Reis,[4] and by the present authors. The Magnus force contributions are identified by Δ for the

Table 2 Comparison of Magnus force predictions[a]

	Magnus contributions				
α, deg	Δ	δP	τ_ϕ	τ_x	Total Magnus coefficient
2	0.000714	...	...	...	0.000714 (Sedney[1])
2	0.000264	0.000439	...	...	0.000703 (Vaughn and Reis[4])
2	0.000482	0.000342	−0.000187	0.0000426	0.000680 (Dwyer and Sanders[2])
4	0.00143	...	...	...	0.00143 (Sedney[1])
4	0.000528	0.000878	...	...	0.00141 (Vaughn and Reis[4])
4	0.00169	0.000598	−0.000348	0.0000714	0.00201 (Dwyer and Sanders[2])

[a] $M_\infty = 2.0$, $R_\infty = 1.74 \times 10^6$, $\omega = 30{,}000$ rpm, $T_\infty = 318°R$, $T_w = 574°R$.

displacement-thickness portion, δP for the radial-pressure-gradient effect, and τ_ϕ and τ_x for the circumferential and streamwise components of wall shear. The streamwise shear stress component τ_x produces a small contribution to the Magnus force, generally about 10% of the contribution of τ_ϕ. However, the other three components are of similar absolute magnitude. The τ_ϕ component is in the opposite direction of the other three contributions, and a significant cancellation effect is shown by the addition of this contribution to the overall Magnus coefficient.

A comparison of the various contributions to the Magnus force given in Table 2 shows vastly different magnitudes, although the total Magnus force coefficients compare well. This agreement in total Magnus coefficients appears, however, to be fortuitous, since the physical basis for the Magnus force is different in each of the analyses. There are presently no available experimental data with which to compare these three results.

Lin and Rubin[3] have calculated the three-dimensional viscous flow over spinning cones for several cone-to-freestream stagnation temperature ratios using a modified boundary-layer technique. They reported Magnus contributions from crossflow shear τ_ϕ and from centrifugal pressure gradient δP, and they estimated the displacement-thickness contribution using slender-body theory. Although their results are for considerably smaller spin rates, 2000 and 4000 rpm, they found also that the crossflow shear and the centrifugal pressure gradient each had a considerable cancelling effect on the other. They also found that the major contribution to the Magnus force came from the asymmetrical displacement thickness for ratios of cone temperature to freestream stagnation temperature near 1.0 (adiabatic wall). The results of Lin and Rubin[3] and of the present authors agree qualitatively.

Figures 6-8 show the Magnus force results of the present analysis for a constant cone temperature of $T_w = 574°$R and a constant freestream temperature of $T_\infty = 530°$R. These conditions should match closely the flight conditions of massive projectiles fired into the atmosphere. Since the wall and freestream temperatures are constant, the ratio of T_w/T_0 varies with freestream Mach number. The Mach 4.0 case is for a very cold wall flow and, consequently, thin boundary layer.

Figure 6 shows that, for small angles of attack, the displacement-thickness contribution and the sum of the other boundary-layer components are of about equal magnitude. At higher angles of attack the displacement thickness contributes much more to the overall Magnus force. Figure 7 shows the effects of high Mach number and a very cold wall. Here, the cancellation of centrifugal pressure gradient and shear is almost complete. Since the displacement-thickness contribution makes up the major portion of the Magnus force, any approximations in calculating this component will be reflected directly in the total Magnus force. The sizes of the three internal boundary-layer components are shown in Fig. 8. These curves are for the same conditions as for Fig. 7. The τ_x component is very small for this case, but the δP and τ_ϕ components are of magnitudes comparable to the displacement-thickness component. These two components are of almost equal magnitude but of opposite sign. Vaughn

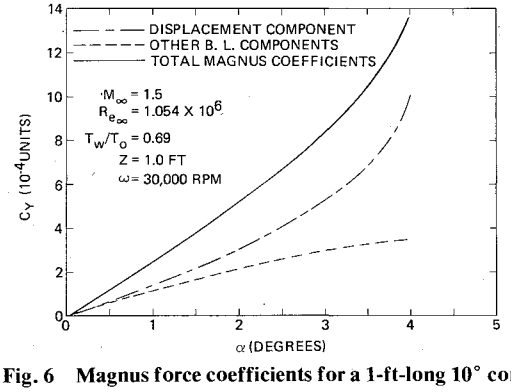

Fig. 6 Magnus force coefficients for a 1-ft-long 10° cone.

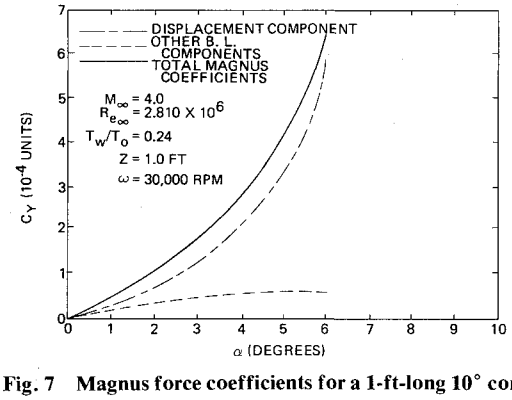

Fig. 7 Magnus force coefficients for a 1-ft-long 10° cone.

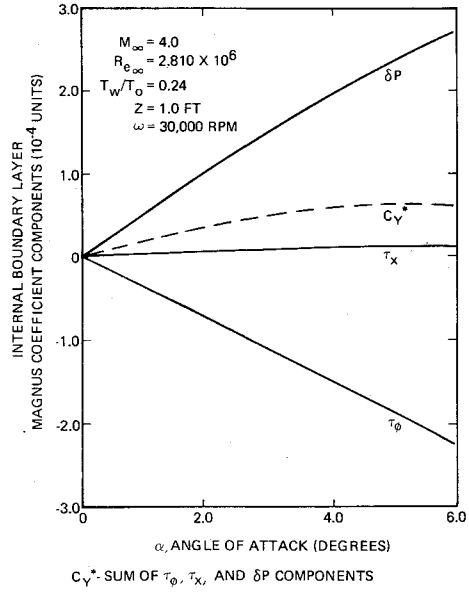

Fig. 8 Internal boundary-layer Magnus force coefficient components and sum for a 1-ft-long 10° cone.

and Reis[4] considered the radial pressure gradient component but not the component due to wall shear. It is clear that, for cases such as in Figs. 7 and 8, a large discrepancy would exist if the wall shear were not included.

Conclusions

A fully three-dimensional calculation of the interaction of the displacement thickness with the inviscid flowfield has been described. It has been shown that this interaction is the physical basis for a major portion of the Magnus force on spinning cones at angle of attack. The techniques employed here are applicable to body shapes other than cones, so long as the inviscid flow is everywhere supersonic. All of the results presented are for laminar boundary-layer displacement thicknesses, but turbulent or transitional boundary layers can be handled easily, so long as a displacement thickness can be defined.

Total Magnus forces are shown for a variety of Mach numbers, wall temperatures, angles of attack, and spin rates. Four components to the Magnus force are calculated in Parts I and II of this paper, and it is shown that a considerable cancellation takes place between the radial pressure gradient and crossflow shear. The total Magnus force seems to agree with two previous calculations,[1,4] but the physical basis for the Magnus force is quite different in each of the theories.

References

[1]Sedney, R., "Laminar Boundary Layer on a Spinning Cone at Small Angles of Attack in a Supersonic Flow," *Journal of the Aero/Space Sciences*, Vol. 24, June 1957, pp. 430-436.

[2]Dwyer, H. A. and Sanders, B. R., "Magnus Forces on Spinning Supersonic Cones; Part I: The Boundary Layer," AIAA Paper 75-193, 1975.

[3]Lin, T. C. and Rubin, S. G., "Viscous Flow Over Spinning Cones at Angle of Attack," AIAA Paper, Palm Springs, Calif., 1973.

[4]Vaughn, H. R. and Reis, G. E., "A Magnus Theory for Bodies of Revolution," Rept. SC-RR-720537, Jan. 1973, Sandia Corp.

[5]Kutler, P., Warming, R. F., and Lomax, H., "Computation of Space Shuttle Flowfields Using Noncentered Finite-Difference Schemes," *AIAA Journal*, Vol. 11, Feb. 1973, pp. 196-204.

[6]MacCormack, R. W., "The Effect of Viscosity in Hypervelocity Impact Cratering," AIAA Paper 69-354, Cincinnati, Ohio, 1969.

[7]MacCormack, R. W., "Numerical Solution of the Interaction of a Shock Wave With a Laminar Boundary Layer," *Proceedings of the International Conference on Numerical Methods in Fluid Dynamics, Lecture Notes in Physics*, Vol. 8, edited by M. Holt, Springer-Verlag, Berlin, 1971.

[8]Abbett, M. J., "Boundary Condition Calculation Procedures for Inviscid Supersonic Flowfields," AIAA Paper, Palm Springs, Calif., 1973.

[9]Jones, D. J., "Tables of Inviscid Supersonic Flow About Circular Cones at Incidence $\gamma = 1.4$," *AGARDograph 137*, 1969.

[10]Moore, F., "Displacement Effect of a Three-Dimensional Boundary Layer," Rept. 1124, 19533, NACA.